

Driveline model calibration and validation in an automotive 4-cylinder Diesel application

N. Andersson¹, T. Abrahamsson²

¹ Volvo Car Corporation, Department of Transmission Engineering
SE-405 31, Gothenburg, Sweden
e-mail: nander17@volvocars.com

² Chalmers University of Technology, Department of Applied Mechanics
SE-412 96, Gothenburg, Sweden

Abstract

We present a computational approach to driveline system simulations that aim to better capture how major system deformation modes vary and interact during operation. A prototype of a downsized front-wheel-drive powertrain was run in a physical rig-test and a nonlinear driveline torsional resonance response could be identified. A large-scale powertrain computational model that combines details of finite element component and multibody system design models was developed and used to simulate the rig-test response. The torsional response was calibrated using one subset of measured data and a complementing subset was used for validation. Simulation results show good qualitative agreement with measured responses. A minor parameter study shows how parameter settings of selected components influence the system normal modes.

1 Introduction

The driveline of a passenger car is a complex and strongly nonlinear mechanical system that transfers and distributes the engine's power to the driving wheels. Together with an attached internal combustion engine it forms the system we here focus on and call the powertrain. The driveline consists of multiple connected subsystems, such as flywheel and clutch, gearbox with differential unit and multi-link driveshafts. Many of these subsystems are themselves complicated constructions' involving flexible rotors, gears and bearings, large deformation springs and drive joints. Load transferring mechanical couplings generally introduce strongly nonlinear elements into the system, such as rotational clearances, uni-directional contacts, friction damping, hardening and softening stiffness. The driveline design, *i.e.* the way these components and subsystems are specified and put together, have shown to have great influence on the complete powertrain's dynamical behaviour and, further, on multiple related vehicle qualities, such as noise and vibrations, driveability and fuel consumption.

Experience-based physical testing in combination with advanced vehicle application tuning has traditionally been the general approach to product development within the automotive industry. However, this becomes harder to accomplish with the introduction of more advanced technologies and overall tougher requirements. Often component development and verification are out-sourced to suppliers external to the company and there is an inevitable risk for late-minute surprises when parallel developments are brought together for final system verification. Driveline vibrational problems sometimes appear and disappear during development tests in rig or vehicle, from one prototype to another or with changing environmental conditions, which altogether indicates that the system is not sufficiently robust to small variations. When new problems appear during hardware calibration (or do not disappear) it is difficult to make a successful recalibration without having a proper understanding of the underlying physical phenomena. Powertrain simulation models are created within the normal product development process to assist in the understanding of critical responses that appear during physical testing and to investigate the

effectiveness of possible upfront design changes to remedy occurring error-states. Intuitive-based simplifications and system linearisations are often used to describe specific system responses. For nonlinear dynamical systems such models tend to have a limited validity in more general situations. For instance they do not capture well how fundamental response modes vary with speed and load over the complete operating range. Also when multiple uncorrelated models exist and represent different views of the same physical system, they may very well come to opposite conclusions on overlapping or closely related issues. Clearly, there is a need to make reliable and consistent assessments of the qualitative dynamical behaviour of powertrain systems. This requires an improvement of existing powertrain simulation models to include a wider range of dynamical phenomena and to increase their range of validity over the complete operating range.

The automotive standard approach to structural dynamics can be said to be the calculation of linear normal modes of an assembly of elastic finite element (FE) models under the assumption of small deformations, which is then followed by a frequency-response calculation using measured or elsewhere estimated external loads. These component models are geometrically detailed and each typically consist of 10-1000 thousands nodes which are created to resolve the dynamics in the range 200-2000 Hz and the corresponding local material stresses. To instead evaluate how the powertrain and driveshafts behave in the large, other complete vehicle mechanical models are built typically using multibody simulation software. These models are made with a clear focus on the quality of driveability, which can be related to powertrain and vehicle normal mode interactions as well as severe transient driveline responses and vibrations in the 2-20 Hz frequency range. These models often have a couple of hundred degrees of freedom (DOF) and consist of multiple rigid bodies connected by one-dimensional visco-elastic components and ideal kinematic constraints. Also, to deliver specific driveline functionality, responsible subsystem developers need to estimate and consider the loading that their designed components experiences during life-long usage. The tightly integrated dual-mass-flywheel (DMF) and clutch subsystems are known to be very central to the resulting torsional vibrations in the drivetrain. They directly experience the peak-loads of the pulsating combustion engine and provide multiple functionalities for reduction of downstream driveline vibrations. Consequently, few-DOF driveline torsional vibration models are developed for design optimisation, having more detailed models of the included arcsprings, [1] and [2]. Due to proprietary rights these models are usually not made available to the driveline system designer in time for design specification.

A vast amount of scientific publications deal with the problem of torsional vibrations related to driveline design, see for example [3]-[5]. In papers like these, driveline system models are often directly represented by one or two rotational DOF, which limits the subsequent analysis to some specific response mode. On the other hand they include strongly nonlinear effects that could be of importance. Analytical modelling and physical reasoning are used together with numerical simulations to point out interesting nonlinear phenomena and evaluate design trends in relation to component parameters. Bourdon, *et.al.* in [6], give an example that shows the importance of modelling the system a bit further. Including fully coupled helical gear forces and nonlinear conical bearings in a FE gearbox model with shafts and casing, they studied the effect of alternative torque directions on the system normal modes. A static torsional tangent stiffness variation of 18 percent was shown between drive and coast conditions and a further general increase of 15 percent was obtained with a rigid gearbox casing. The corresponding eigenfrequency distributions in linearised states were quite different, all due to load redistributions in bearings and housing structures. More recent modelling of a complete internal combustion engine can be seen in the paper by Novotny and Pistek, [7]. They include detailed component models of the cranktrain, valvetrain, gear timing mechanism and fuel injection pump and point out the importance of understanding system dynamical interactions.

In this paper the central issue is calibration and validation of a newly developed powertrain simulation model that, better than before, treats undesirable nonlinear system behaviour and has a potential to unify good use of virtual simulations over the complete automotive design process. We compare basic qualities of simulated and measured torsional dynamic responses of an equally new front-wheel-drive four-cylinder Diesel application. Measured signals of shaft angular velocity were obtained from a physical rig-test, in which a critical nonlinear resonance was identified during slow speed-sweeps at different levels of loading.

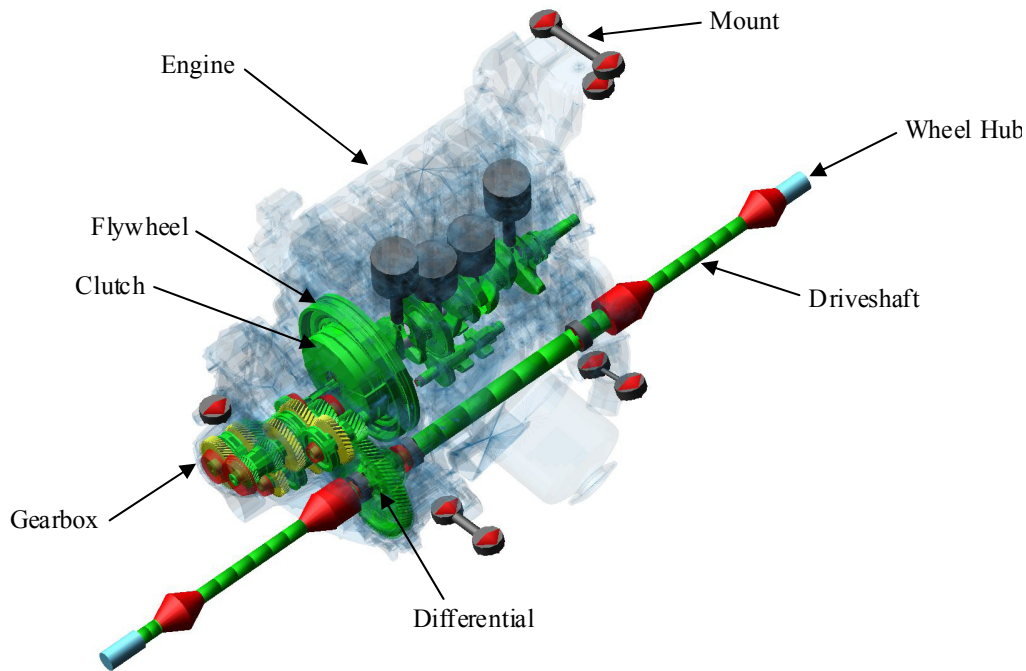


Figure 1: Overview of the powertrain computational model. The engine block and gearbox casing structures are made transparent to show more of the internal rotating parts.

2 Modelling approach

We use linear reductions of all major elastic structural components together with multiple nonlinear parameter connection models. This reflects our experience that much of the responses seen in the driveline are related to how the nonlinear joints couple the flexible structures of the system. Accurate stiffness and inertia distributions as well as cross-coupling terms between interface DOF, due to large angular displacements, gyroscopic forces, *etc.*, are central for a better capture of system interactions occurring in three-dimensional physical space. For better usage of virtual tools in the design process it is important that the system model can function as a unifying platform for design analysis simulations, from early conceptual phases to final verification and physical rig-testing. It should also support system requirement cascading into balanced component requisites. For this we have specified and implemented an interface-based model structure, where each subsystem's physical connection points are directly represented, which facilitates successive model refinements and working with variable system borders. This combines the details of FE analyses with the system design approach of multibody dynamic simulations. We use a constrained general state-space formulation as implemented in the commercially available software-suite ADAMS [8]. The resulting set of nonlinear first-order differential and algebraic equations is solved by numerical time integration using a predictor-corrector approach. The possibility to effectively combine largely rotating flexible parts with general state-space models is an attractive feature of this code. Further it has proven to solve numerically stiff integration problems well; it allows linearisation and computation of normal modes and state matrices of the system at any specified moment in time.

In the following, we give a description of the powertrain model's main characteristics. An overview of flexible and rigid structural components of the model is shown in figure 1. The engine block with auxiliary structures, mounting brackets, transmission and clutch housings (all dimmed) are modelled as linear elastic bodies. This also applies to the crankshaft and the flywheel's primary side, gearbox shaft assemblies and differential housing with ring gear wheel. Generally, we use tetrahedral FE component models created using established engineering software, [9] and [10]. Non-structural masses, springs and dampers that are expected to influence the system dynamics are modelled using the corresponding standard elements (CONM2 and CELAS elements in NASTRAN [11]). Rigid elements are used as fasteners and to distribute point loads (RBE2 and RBE3 in NASTRAN, respectively). Multiple component

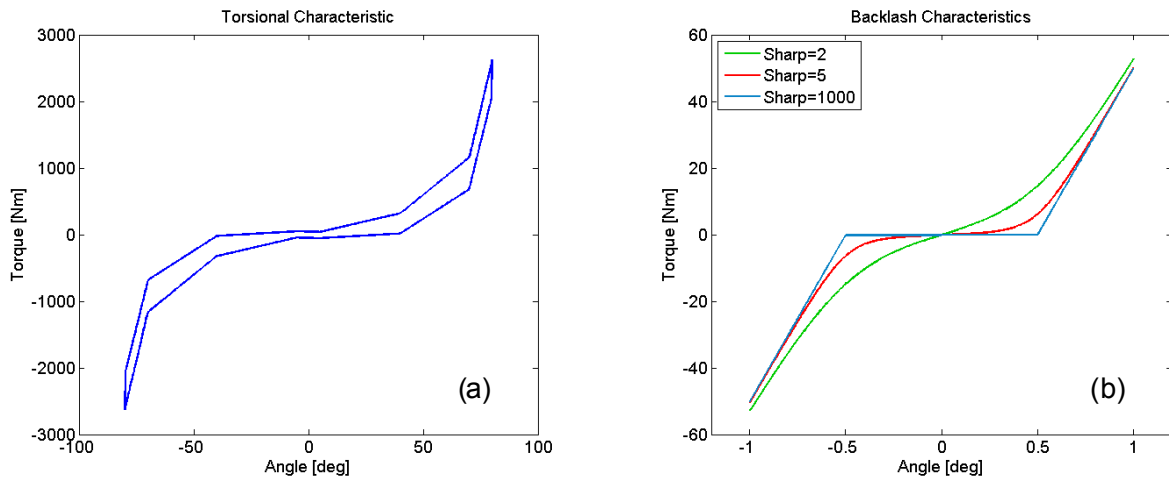


Figure 2: Qualitative load versus deformation model examples: DMF torsional characteristics is shown in (a) and rotational backlash characteristics for three different sharpness factors in (b).

models are then attached to form larger structural blocks that internally are assumed to behave linearly. Trusted joint-modelling techniques are used, where RBE2 or RBE3 elements are combined to give a reasonable equivalent macroscopic stiffness. All parts include inertial and stiffness cross-coupling terms. Pistons and connecting rods, multiple clutch and flywheel parts, gear wheels and synchronisation are the major components that are modelled more schematically using combinations of rigid and scalar spring-damper elements. Still they uphold a node-interface that fit into the specified modelling structure. Shafts, gears, flywheel, *etc.*, rotate during simulation to allow for gyroscopic effects. To obtain a numerical solution of the system response within a reasonable computational time, model reduction techniques must be utilised. ADAMS uses the well-known Craig-Bampton method, which is described in [12].

Connections are modelled as forces and moments acting between two coincident six-DOF interface nodes. Typical driveline connections are bolted and splined joints, gears and bearings. Most of these are designed to function as ideal joints, where other relative motions and secondary friction forces are small. Therefore, unless otherwise indicated, we generally assume that basic kinematic constraints, like fixed or revolute joints, are adequate. Other suspected, or known-to-be, critical joints for which relevant data are available are modelled to deform linearly or nonlinearly using FIELD or BUSHING statements in ADAMS, respectively. Examples of the first type of such deforming joints are the crankshaft's main bearings, which are modelled using a full linear coupling matrix between interface nodes. This is still a simplified representation of the true bearing dynamics, but according to [7] there are no significant benefits for the cranktrain dynamics to increase its complexity into a full elasto-hydrodynamic solution. An example of the second type is the axially preloaded plain bearing between the flywheel's primary and secondary parts that deforms nonlinearly in bending and is modelled by uncoupled and load-dependent stiffnesses.

More specifically for the gearbox, we use a two-noded tapered roller bearing model, developed by Houpert [13], that couples pair of five DOF between the shaft and housing structures. It uses bearing macro data to calculate the resulting nonlinear displacements and reactions between inner and outer rings, considering internal geometry, roller kinematics and Hertzian contacts. The driving action and reaction torque between the flywheel's primary and secondary parts are modelled using a qualitative description including elastic, viscous and hysteretic force components. An example of such an arcspring stiffness curve is shown in figure 2a. Attached to the flywheel's secondary side are a number of centrifugal pendulum vibration absorbers that act to further mitigate torsional fluctuations of a tuned rotational order [14]. These pendulums are parametrically modelled as hinged rigid rods whose centre-of-gravity position is constrained to follow a specified curve-type. The modelled friction lamella torque can generate dynamic stick-slip behaviour using the slip-speed dependent Coulomb coefficient of the FRICTION statement in ADAMS. In addition, the clutch model is equipped with optional torsional springs between its outer and inner parts. A full set of helical gear contact forces and two resulting moments are transferred between two separated interface nodes located at gear wheel centres. Macro-geometrical gear data and relative gear

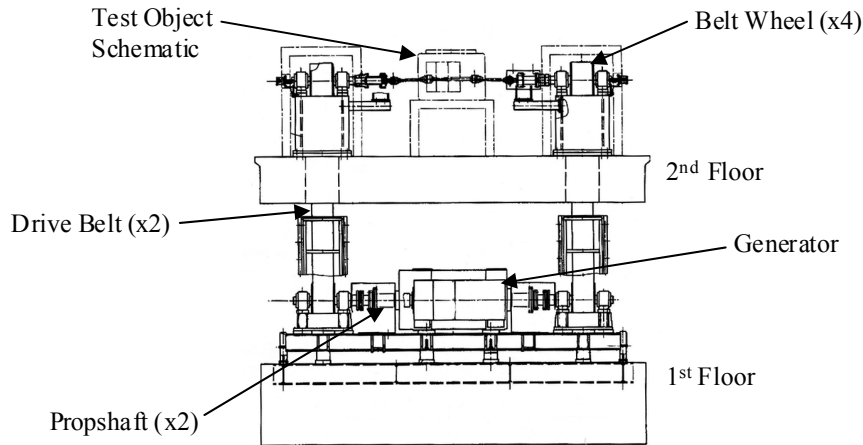


Figure 3: Test-rig schematics from the maintenance manual. Each driveshaft is coupled to a belt wheel and, in turn, to another such wheel located one floor down by means of a drive belt. The two belt wheels below are then connected by two propshafts and a central breaking generator, closing the torque-split.

wheel displacements (three translations and two rotations) are used together with standard formulas for cylindrical gear kinematics to calculate the forces, [15] and [16]. Differential gear contact forces are calculated similarly, but instead using the corresponding formulas for conical gears [17] and only one relative shaft displacement (the principal rotational). Conical gear wheels are included as separate rigid parts, which are hinged relative to the differential housing and driveshaft inner-ends, respectively. Backlash and teeth rotational contact stiffness are modelled for all gear pairs in the driveline. This is accomplished by modifying the connection forces and moments by a parametric arctangent function (see figure 2b). The user determines the strength of individual discontinuities by specifying values of included sharpness factors, lash angles and asymptotic stiffnesses. Driveshafts are modelled with multiple BEAM statements in ADAMS, which transmit a full set of forces and torques in accordance with nonlinear Euler-Bernoulli theory [8]. We use model parameters corresponding to physical dimensions, configuration angles and material data of the shafts to facilitate design studies. Multi-link driveshafts include one or more ideal kinematic joints of optional type, like combinations of translational and constant velocity joints. As with gears, rotational clearances and local torsional contact stiffness of joints are incorporated in terms of arctangent functions.

Combustion pressure loading is applied by pairs of action and reaction forces between pistons and cylinder heads, as individual function of crankshaft angle and throttle position, resulting in a correct firing sequence. A virtual powertrain-rig attached to the driveshaft's outer-ends is used to break the system, like in physical rig-tests. Finally, external ground-reactions also results from large displacing rubber mounts, corresponding to the powertrain and driveshaft connections to surrounding vehicle or rig-systems.

3 Physical testing

To obtain real-life test data for validation, a prototype of a downsized front-wheel-drive powertrain was run in a physical rig-test. In brief overview, the tested powertrain consisted of a four-cylinder Diesel engine, DMF with centrifugal pendulum vibration absorbers, a stiff mechanical clutch and six-speed manual transmission with the fourth gear in driving position, as well as driveshafts with lengthwise self-adjusting constant velocity joints. When mounted in the rig, the system is attached to a stiff metal frame via its rubber mounting system, which in turn is bolted to the floor of the building. The system load is generated by the tested combustion engine and regulated by adjusting its throttle. By engaging the mechanical clutch the heavily fluctuating engine torque enters the driveline through the flywheel, loads the gearbox's internal components, splits through the differential unit, and goes into the test-rig terminal break unit via the outer-end of the driveshafts, as seen in figure 3. The breaking torque from an electric

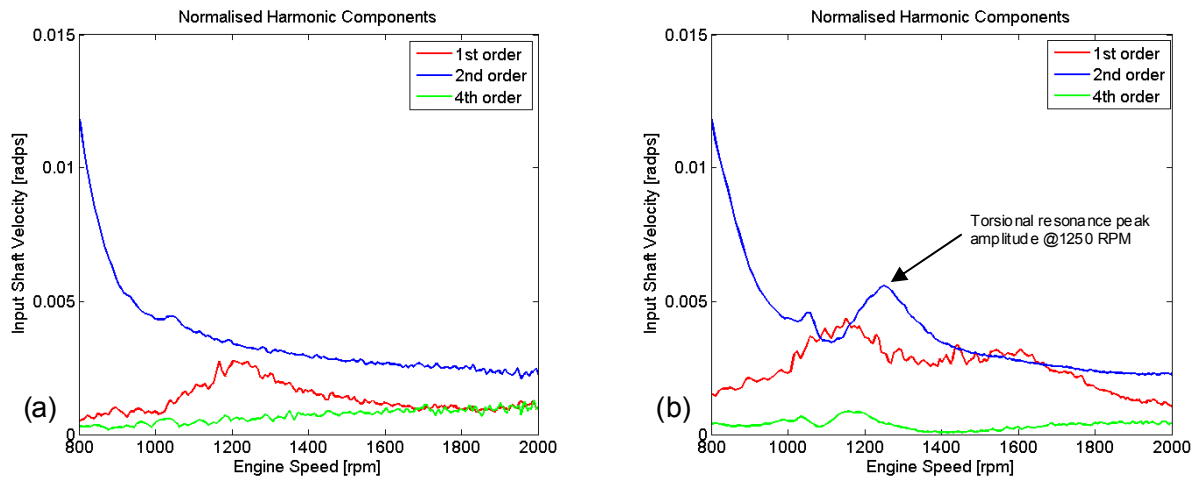


Figure 4: Harmonic order-tracks from gearbox input shaft velocity response: (a) shows response at 20% throttle and (b) at 40% throttle. A critical 2nd order resonance appears at high loading around 1250 RPM. Contributions from other orders are insignificant.

generator regulates the system's rotational speed. In our rig-tests, the engine was set to make multiple slow speed-sweeps over the range 800-4000 crankshaft revolutions per minute (RPM). Each run was made with the same constant speed-rate of 14 RPM per second, but with a different constant throttle position.

To evaluate the torsional dynamical response of the system under operating conditions, an inductive pulse-generating system was used. In short, it calculates the time-average angular speed of the rotating part from the time between successive pulses and the angular distance between the pulse-generators. Typically, the gear tooth flanks of a fixed gear wheel are used as pulse-generators. For more details about the function of the measuring system the reader is referred to [18]. For the test, three pickups were mounted at different locations along the driveline. The first one was placed on the clutch housing, close to the flywheel's primary part. The second pickup was located close to the 6th pinion gear at the end of the gearbox input shaft. The third measured signal was obtained from the gearbox's ring gear wheel. By this arrangement, according to the Shannon sampling theorem [19], we always resolve frequency content up to at least 185 Hz when the engine runs above 800 RPM, see table 1. The rig's break torque was also recorded.

Fourier transformation is used to decompose the measured angular velocity signals into its harmonic components [20], however not valid for non-stationary conditions like our speed-sweeps. We account for the constantly changing rotational speed by using constant angular sampling and apply the transform to angular-domain data. However, even for very slow sweep-rates at constant throttle, the rapid changes of engine torque amplitudes are likely to introduce leakage-effects into the analysis. An interesting discussion of the limitations of Fourier order-tracking applications is given by Blough in [21]. The response data were normalised with the average breaking torque before analysis. This normalisation makes it possible to recognise nonlinear response characteristics, since an ideal linear system would show identical normalised responses for any load level. In figure 4, normalised order-tracks from slow speed-sweep tests at different load levels are shown. We generally see large vibration amplitudes in the speed range 800-1000 RPM, which are related to the fundamental torsional resonance intentionally placed below

Pulse generator	Gear ratio	Pulses per revolution	Max order resolution	f_{\max} @ 800 RPM	f_{\max} @ 4000 RPM
Starter ring	1	144	72 th	959 Hz	4800 Hz
6 th pinion	1	37	18.5 th	246 Hz	1233 Hz
Ring gear	2.95	82	41.5 th	185 Hz	926 Hz

Table 1: Summary of measuring apparatus order and frequency limits. Max frequency resolution values refer to crankshaft rotational speed.

normal service idle speed as part of the DMF design strategy. However, the most noticeable difference between responses at 20 and 40 percent throttle is a possible nonlinear increase of gearbox input shaft vibration amplitude around 1250 RPM. This is critical since it is in the speed-range in which the engine should be driven to obtain optimal fuel consumption. Thus this resonance is at the heart of the conflict between reduced emissions and vehicle noise and vibrations.

4 Numerical simulations with calibration and validation

Numerical simulations provide possibilities to replicate and predict the response of a real-life powertrain system. This could reduce the need for expensive hardware prototypes and overcome practical difficulties related to physical testing. Other difficulties instead need more attention. For example, many parameters must be included and given relevant numerical values to successfully model a real-world system. Ideally these would represent only physical properties that were all well-known and documented. This is never the case though, due to simplifications made on some level. Therefore model parameter calibration is required to validate the model. In order to assess the parametric influence on critical system deformation modes, a series of fractional factorial experiment, as described in for example [22], was set up and executed. In each experiment the powertrain system runs from pre-set initial conditions until steady-state response is reached where a linearisation of the system is performed and followed by a calculation of normal modes and frequencies. The parameters of the study were the DMF torsional stiffness, the input shaft stiffness, the driveshaft stiffness and the rig polar inertia, which were considered to be most important in this study. The chosen parameter values correspond to existing shaft design solutions, high and low system loading of the DMF arcspring and alternative conditions at the boundary between the driveshaft and the rig, see table 2.

The linearisation of the strongly nonlinear system under operation is not unique. This is partly due to the strong fluctuations of the torque from the combustion engine. These fluctuations amplitudes are of a magnitude exceeding the time average torque. Over a principal excitation time-period the springs of the DMF will work over both the stiff and soft parts of its stiffness domain, whereas momentarily, it is in a single position on either the stiffer or softer state. Since linearisation is made at a specific state, the calculated system normal mode frequencies correspond to that state only. Thus the calculated linear normal modes are expected to be time-dependent, fluctuating between extreme states. Therefore during the parameter study, attention was given to drive the system to steady-states of small amplitudes, where more distinct linearisations could be made and the corresponding modes and eigenfrequencies calculated. Shapes of torsional modes were correlated by visual inspection of animations. The results from the parameter study is summarised in figure 5, which shows that most system eigenfrequencies below 150 Hz vary with the chosen parameter values. Only a cluster of powertrain rigidbody modes between 6-13 Hz is

Experiment #	Arcspring	Inputshaft	Driveshaft	Rig
	stiffness	stiffness	stiffness	inertia
	+: 26 Nm/deg -: 6 Nm/deg	+: 1.25E -: 0.75E	+: 1.25E -: 0.75E	+: 10 kg m ² -: 1.5 kg m ²
1	—	—	—	—
2	+	—	—	+
3	—	+	—	+
4	+	+	—	—
5	—	—	+	+
6	+	—	+	—
7	—	+	+	—
8	+	+	+	+

Table 2: Specification of fractional factorial experiment with four parameters. Low and high (-/+) parameter values used represent possible component design solutions. E in table header refers to nominal Young's modulus value of steel (individual for different shafts). Static load and steady-state speed were 100 Nm and 1000 RPM, respectively.

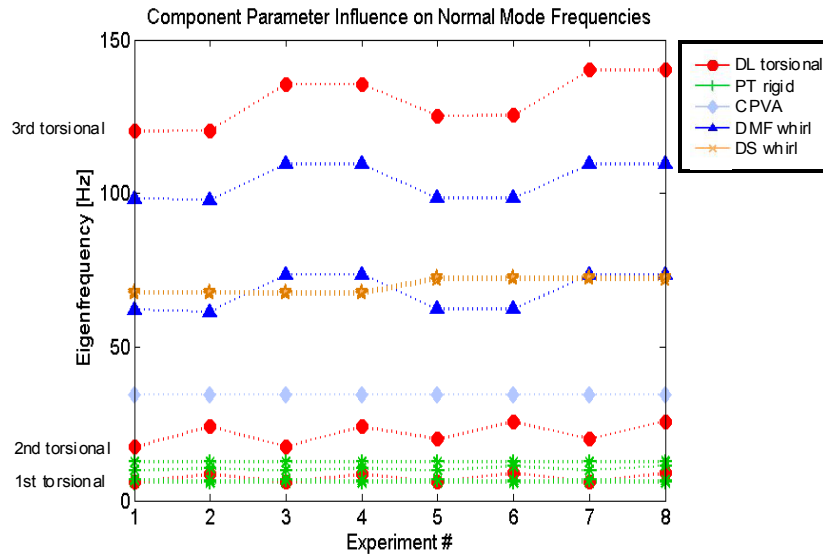


Figure 5: Overview of changes in normal mode frequencies due to parameter variations specified in table 2. Abbreviations are used for driveline (DL), powertrain (PT), centrifugal pendulum vibration absorber (CPVA), dual mass flywheel (DMF) and driveshaft (DS).

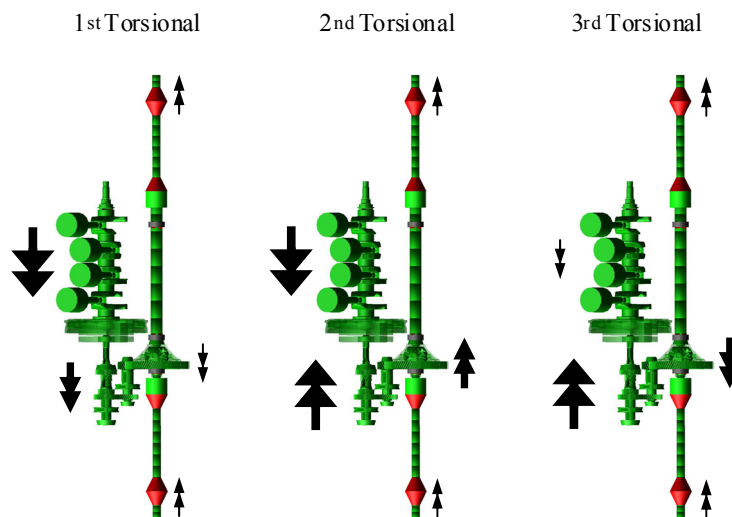


Figure 6: Illustration of the torsional normal mode shapes of main interest. A double-arrow indicates the direction of relative rotation of the adjacent structure and the size of the arrow reflects the corresponding maximum vibration amplitude.

largely unaffected. It was found that the arcspring stiffness shows a major influence on the second torsional mode frequency and the gearbox stiffness strongly affects both the third torsional and the DMF whirling mode frequencies. The driveshaft stiffness influence all torsional modes, but to a lesser extent. With this set-up, the rig inertia shows no significant influence on any mode in the range 5-150 Hz. The three torsional modes of main interested are illustrated in figure 6. The system modes and engine excitations also vary with operational speed. Gyroscopic forces, see for instance [23], cause that the flywheel's tilting mode eigenfrequencies split and vary in frequency with increasing crankshaft speed. This is seen in the Campbell plot presented in figure 7, which give an overview of possible dynamical resonances.

To help in comparing simulated and measured responses and to quantify the effect of successive parameter changes, a deviation metric was defined. The modelling purpose is to determine if there is a

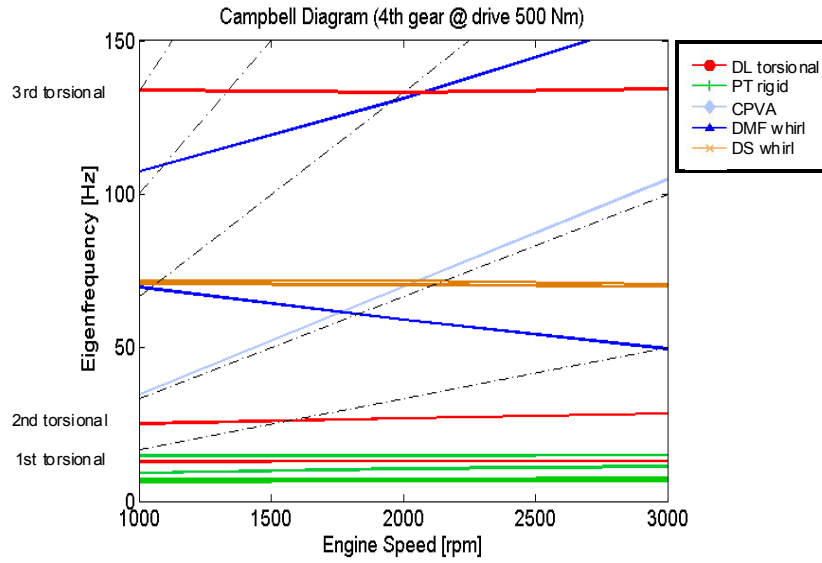


Figure 7: Campbell diagram that shows how system linear modes and crankshaft order related excitation vary with engine speed. Dash-dotted lines correspond to crankshaft rotational orders.

system resonance and, if so, at what frequency it occurs and, further, to follow how it changes with load and speed. This is in contrast to precisely finding the correct amplitude and phase of a specific time-response. Therefore, we choose to focus more on overall similarity between responses. More specifically, we intend to compare shapes of principal harmonic order-tracks of measured and simulated responses. Consider such an order-track, like the second-order curve in figure 4b, which is defined by a pair-sequence of amplitude and speed values, u_j and v_j respectively, where $j = 1, 2, \dots, J$ is the sample-index. For comparison, every sequence must have the same number of samples, J , which is achieved by resampling and interpolation whenever necessary. We use available functions within MATLAB [24] for that. First, we define the corresponding amplitude vector as

$$\mathbf{u} = [u_j] \tag{1}$$

A deviation vector, $\boldsymbol{\gamma}$, is defined as the point-wise difference between measured and simulated amplitude vectors, ${}^M\mathbf{u}$ and ${}^S\mathbf{u}$, respectively.

$$\boldsymbol{\gamma} = {}^M\mathbf{u} - {}^S\mathbf{u} \tag{2}$$

The magnitude of the deviation vector reflects the overall discrepancy and a perfect match will thus render $\boldsymbol{\gamma} = \mathbf{0}$. This deviation vector is then adjusted to have a zero-mean and, consequently, the absolute response level is not considered further. The components of this adjusted deviation vector, $\tilde{\boldsymbol{\gamma}}$, are defined as

$$\tilde{\boldsymbol{\gamma}}_j = \boldsymbol{\gamma}_j - \bar{\boldsymbol{\gamma}} \tag{3}$$

where the average error, $\bar{\boldsymbol{\gamma}}$, is given as follows.

$$\bar{\boldsymbol{\gamma}} = \frac{1}{J} \sum_{j=1}^J \boldsymbol{\gamma}_j \tag{4}$$

Secondly, to better track resonance frequencies of the system, we include a measure of how close in relative speed a simulated peak-response is to the corresponding one identified in the physical test. Therefore, in the same spirit, another error metric, δ , is formed as the difference of measured and simulated speed values

$$\delta = {}^M v - {}^S v \quad (5)$$

where, ${}^M v$ and ${}^S v$, are two extracted single speed values, each in couple with the maximum peak-value of the corresponding order-track-curve, as indicated in figure 4b. Sign-changes of the curve's slope are used to locate peak-value candidates. Next, equations (3) and (5) are combined for two different load cases into the vectorised weighted error vector, $\boldsymbol{\varepsilon}$, defined by

$$\boldsymbol{\varepsilon} = \left[\begin{matrix} \text{I} \tilde{\gamma}_j w_1 & \text{I} \delta w_2 & \text{II} \tilde{\gamma}_j w_3 & \text{II} \delta w_4 \end{matrix} \right] w_5 \quad (6)$$

where the error-superscripts, I and II, correspond to the low and high load-levels of our rig-tests, respectively, and the scalar weights, w_1 , w_2 , w_3 and w_4 , are chosen so that each weighted error component is of equal magnitude and the following equality holds true.

$$w_1^2 + w_2^2 + w_3^2 + w_4^2 = 1 \quad (7)$$

Finally, the objective function used in evaluation is defined as the scalar quadratic error given.

$$\phi = \boldsymbol{\varepsilon}^T \boldsymbol{\varepsilon} \quad (8)$$

To facilitate the comparison between the nominal and calibrated models, the remaining weight, w_5 , is adjusted to give $\phi = 1$ for the nominal case. This way, any improvements after calibration will correspond to an objective function value less than unity.

To evaluate the harmonic components of the discrete time signals from simulations, we use a linear regression analysis. This simplifies the process of extracting integer-order components as well as checking both signal error and stationary. We use up-sampling and interpolation techniques to obtain an integer number of samples over the longest time-period of interest (the half-order component) at the period-average speed. We further assume that each up-sampled response value, $y(t_n)$, can be written as a summation of complex exponential terms, as follows.

$$y(t_n) = x_0 + x_1 e^{i\Omega_0 t_n} + x_2 e^{i2\Omega_0 t_n} + \dots + x_p e^{ip\Omega_0 t_n} + r(t_n) \quad (9)$$

Here the discrete time $t_n = t_s n$, where t_s is the sampling time increment and $n = 0, 1, \dots, N-1$ enumerate every sample in the sequence. Further, Ω_0 is the chosen fundamental harmonic angular frequency, $p = 0, 1, \dots, P-1$ are the integer order-multiples included in the finite series representation, x_p are the corresponding complex harmonic amplitudes and $r(t_n)$ is the residual term. Written on matrix form equation (9) becomes

$$\begin{bmatrix} y(t_0) \\ y(t_1) \\ \vdots \\ y(t_{N-1}) \end{bmatrix} = \begin{bmatrix} 1 & e^{i\Omega_0 t_0} & e^{i2\Omega_0 t_0} & \dots & e^{i(P-1)\Omega_0 t_0} \\ 1 & e^{i\Omega_0 t_1} & e^{i2\Omega_0 t_1} & \dots & e^{i(P-1)\Omega_0 t_1} \\ \vdots & \vdots & \vdots & \ddots & \vdots \\ 1 & e^{i\Omega_0 t_{N-1}} & e^{i2\Omega_0 t_{N-1}} & \dots & e^{i(P-1)\Omega_0 t_{N-1}} \end{bmatrix} \begin{bmatrix} x_0 \\ x_1 \\ x_2 \\ \vdots \\ x_{P-1} \end{bmatrix} + \begin{bmatrix} r(t_0) \\ r(t_1) \\ \vdots \\ r(t_{N-1}) \end{bmatrix} \quad (10)$$

or, in short,

$$\mathbf{y} = \mathbf{A}\mathbf{x} + \mathbf{r} \quad (11)$$

where \mathbf{y} and \mathbf{r} are N -vectors, \mathbf{x} is a P -vector and \mathbf{A} is a $N \times P$ matrix. Then, assuming that the residual vector, \mathbf{r} , is small we solve for the coefficient vector, \mathbf{x} , that give the least squared difference between the subspace projection, $\mathbf{b} = \mathbf{A}\mathbf{x}$, and the sample vector \mathbf{y} . The resulting complex coefficients are given by equation (12), where superscript, H, is the Hermitian transpose.

$$\mathbf{x} = (\mathbf{A}^H \mathbf{A})^{-1} \mathbf{A}^H \mathbf{b} \quad (12)$$

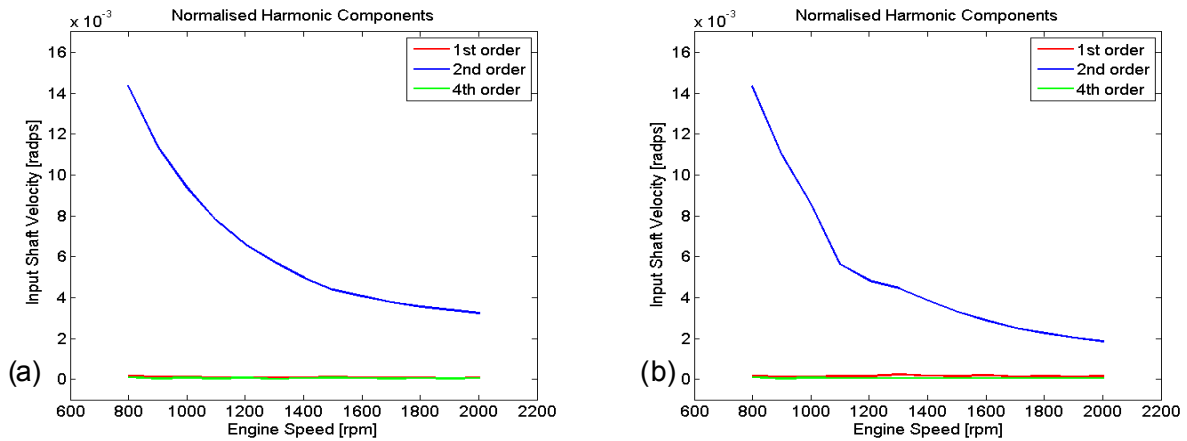


Figure 8: Uncalibrated gearbox input shaft steady-state normalised response order-tracks for low (a) and high (b) loading, respectively. The resonance seen in rig-test is not captured here, see figure 4b. Contributions from other orders are insignificant.

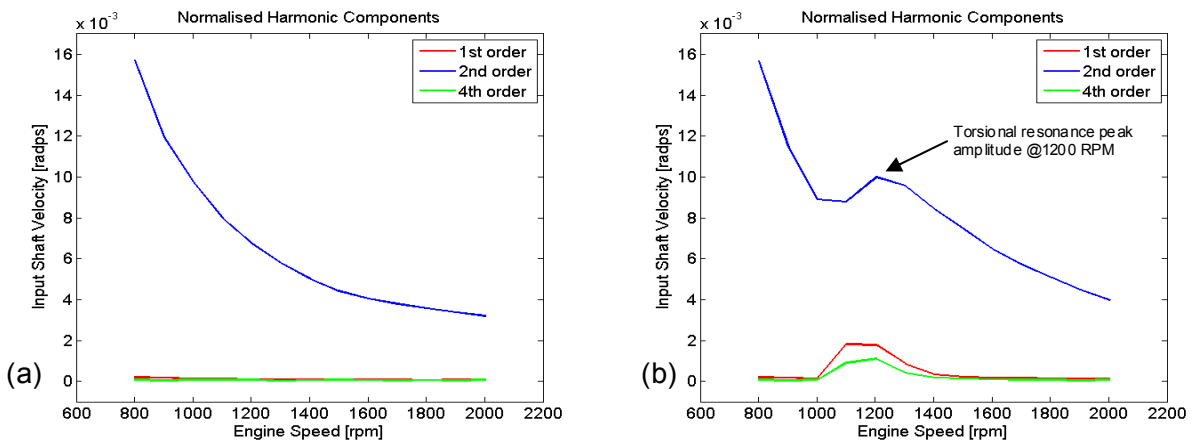


Figure 9: Calibrated gearbox input shaft steady-state normalised response order-tracks for low (a) and high (b) loading, respectively. A resonance corresponding to the one in rig-tests is seen here at 1200 RPM, cf. figure 4b. Contributions from other orders are insignificant.

Response simulations for model calibration were performed and equations (9)-(12) were used to calculate the harmonic amplitudes for every steady-state speed by taking the magnitude of the complex coefficients. The resulting order-tracks from the simulated and normalised steady-state response curves with the nominal model parameter values, corresponding to the ones obtained from the physical speed-sweep tests presented earlier, are given in figure 8, where the objective function of equation (8) evaluates to a unit-value. Burdened by long simulation times, it was necessary to abandon the idea of using continuous speed-sweeps in order to complete the calibration work within reasonable time. Instead we use steady-state simulations at discrete engine speeds. For the same reason, strategies like run-many-cases or gradient-based optimisation are considered too time demanding for calibration simulations. A more practical engineer-in-the-loop approach was adopted where the objective function is evaluated and the next parameter updates are chosen based on the previous outcomes and with the intent of finding a better value the next time. This is repeated until a satisfactorily match between physical and virtual tests is obtained. For the evaluation it was assumed that the effect of the slow sweep-rate used in the physical tests is insignificant for the comparison with steady-state data. Guided by the results from the parameter study, focus was mainly put on testing different arcspring characteristics. The final result of the calibration is shown in figure 9, where the objective function of equation (8) evaluates to a value of 0.827. Clearly the calibrated model generate a resonance around 1250 RPM and 40 percent throttle, which is not seen with the nominal set of parameter values. For validation the same objective function is evaluated as in the

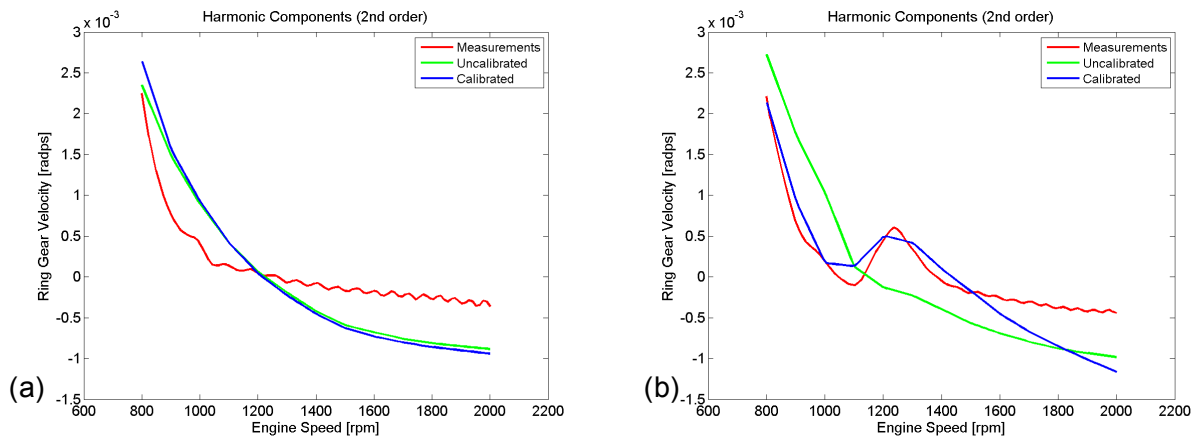


Figure 10: Direct comparison of gearbox ring gear wheel steady-state normalised response order-tracks, corresponding to low (a) and high (b) loading, respectively.

calibration work. This time around, the results from the differential ring gear wheel are used instead. For the three cases: physical testing, simulation with uncalibrated (nominal) model and simulations with the calibrated model, a direct comparison of the adjusted second-order response curves are given in figure 10. The objective function here evaluates to unit-value for the uncalibrated model and to 0.759 for the calibrated model.

5 Concluding remarks

As previously mentioned, the nonlinear response seen in figure 4b is considered critical for vehicle noise and vibrations and the objective of the calibration work was therefore set to tune the model to behave similarly in this respect. Initially we noticed that the measuring points located at the gearbox input shaft and ring gear wheel registered a resonant response around 1250 RPM, whereas the one at the flywheel's primary part did not. Moreover, the flywheel's nominal quasi-static torsional characteristic curve has a strong discontinuity at about 40 degrees angular deformation (*cf.* figure 2a), which corresponds well to the deformations seen in simulations, see figure 11a. Also, the resonant phenomenon was not seen at all in other complementing tests, where the only intended difference was that the DMF-parts were locked together to prohibit loading of the arcsprings (these tests are not necessary for the included results and are not mentioned further here). Altogether the critical response seems to be strongly related to arcspring nonlinearities. Based on this and results from the parameter study, where the arcspring stiffness value seems to control the second torsional mode frequency, the calibration hypothesis used was that the arcspring effective stiffness increase during operation in order for the second torsional mode to be excited by the engine torque around the speed of 1250 RPM.

Generally, the model probably has too low system damping compared to the physical system, since the physical driveline includes grease and other lubricants that are not properly accounted for. Under these conditions, the model's low-speed response amplitudes show a high sensitivity. The arcspring torsional elastic stiffness and its hysteretic damping are found to have major effects on the system response, but also the driveshaft and gearbox effective stiffness are seen to influence. Whether or not, and for what engine speed, a system resonance occurs strongly relate to the operating conditions of the arcspring. Specifically, the stiffness-ratio between stiffer and softer linear elastic parts and the location of the corresponding vertex-point, in combination with the time-averaged value of the external loading, seems to be important for the location of the resonance. Two simulated examples of arcspring steady-state responses are given in figure 11. The calibrated resonant response was obtained by scaling the stiffer elastic part of the arcspring characteristic curve by a factor of approximately 3.4. We found similar behaviours for scale factor values greater than approximately 2, but not for softer arcsprings than that. No corresponding resonance was seen in the simulated speed-range using a single stiff and all-over linear arcspring. As reported, in for example

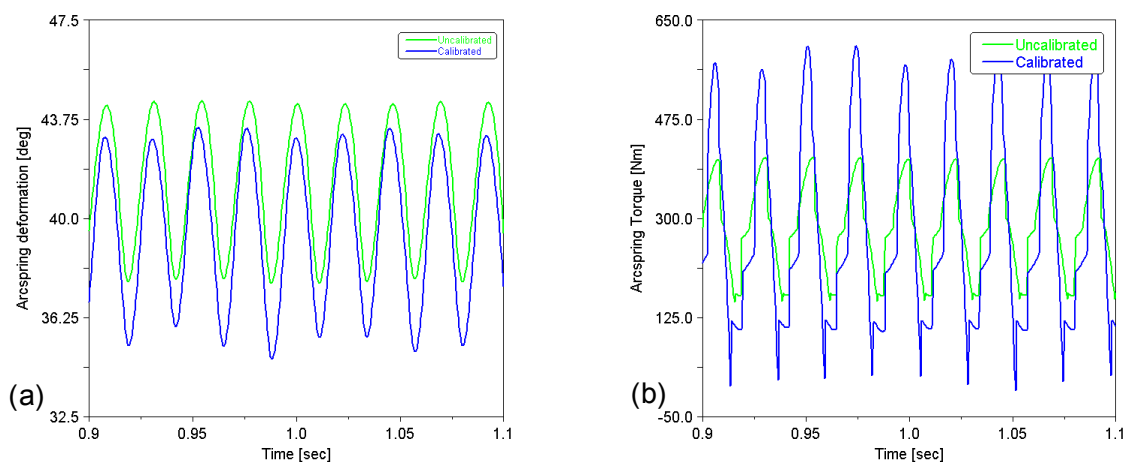


Figure 11: Simulated DMF steady-state time-responses at 1300 RPM and high loading. (a) shows the arcspring angular deformation and (b) shows the corresponding torque. No normalisation applied here.

[1] and [2], it seems reasonable to expect such operational stiffening due to geometrical, centrifugal and frictional effects. Lower levels of arcspring damping results in subharmonic responses as described in [4] and [5]. The occurrence of these and other quasi-stationary responses, which do not settle to steady-state even for long simulations (up to 25 seconds), are noted but not further analysed here.

In the parameter study, rig inertia showed no influence on the calculated eigenfrequencies under controlled speed conditions. However, in other response simulations the torsional resonance around 1250 RPM is found also to depend on the driveshaft boundary conditions. Using an uncontrolled static break-torque, the resonance occurs for rig inertias corresponding to the total inertia of the physical rig, whereas it does not occur if only a significantly smaller inertia is used (comparable to a pair of wheels). This indicates that the driveshaft boundary conditions are significant for the system dynamics and questions the relevance of some existing development tests?

Worth mentioning is also the importance of modelling kinematical couplings. By the introduction of a nonlinear kinematical formulation between helical gear wheels and over conical bearings, we found that the effective torsional stiffness of the complete gearbox decreased a lot, towards a more realistic value. Previously, without these couplings between rotational and translational displacements, each selected gear state required different and somewhat unphysical component stiffness parameters in order to give a reasonable system torsional stiffness. With these couplings, calibration is still required but parameter values remain in a more feasible range and show less load case dependency.

All in all, the system is found to be sensitive to variations in load, speed and damping, which fits the description of the physical system given in the introductory chapter rather well. Based on the overall system behaviour after calibration we conclude that the driveline model successfully reproduce a similar nonlinear torsional resonance as seen around 1250 RPM in rig-tests. Specifically based on the reduced value of the defined objective function, in going from the uncalibrated to the calibrated model, we can say that the model shows good qualitative agreement with measured responses and we consider the powertrain system model to be valid for this torsional response mode.

The list of suggested improvements is of course long and cannot be given in its full. However, the strong influence of the simplified arcspring model parameters on the system response indicates that the dynamical description of the arcsprings is an important matter that needs further attention also for driveline system developers. To improve the prediction quality it is probably critical to use a more physical spring model. Further, to expand the system model's range of validity and to relate different types of responses to each other, the powertrain model should be further used and compared to other physical tests. To this end, to facilitate future calibration work, it is recommended that, during physical testing, the effective cylinder pressure is measured with correct individual phasing. This will eliminate uncertainties of external loading between physical and virtual tests. Also, the assumption made here that slow sweep-rates only have a negligible effect on system response was found to be not all good. Transient effects are

difficult to distinguish from effects due to changes of model damping and steady-state testing is recommended to simplify subsequent analyses as much as possible.

Lastly, to be able to make better predictions during conceptual design analysis and to facilitate robustness evaluation by extensive parameter variations, future work in the field of model-order reduction is planned.

Acknowledgements

This work is financed by Volvo Car Corporation and Energimyndigheten.

References

- [1] A. Kooy, A. Gillmann, J. Jäckel, M. Bosse, *DMF - Nothing new?*, 7th LuK Symposium, LuK (2002), pp. 5-14.
- [2] U. Schaper, O. Sawodny, T. Mahl, U. Blessing, *Modeling and torque estimation of an automotive Dual Mass Flywheel*, American Control Conference (2009), pp. 1207–1212.
- [3] J. Wang, R. Li, X. Peng, *Survey of nonlinear vibration of gear transmission systems*, ASME Applied Mechanics Reviews, Vol. 56, Issue 3, American Society of Mechanical Engineers (2003), pp. 309-329.
- [4] T. C. Kim, T. E. Rook, R. Singh, *Super- and sub-harmonic response calculations for a torsional system with clearance nonlinearity using the harmonic balance method*, Journal of Sound and Vibration, Vol. 281, Elsevier (2005), pp. 965-993.
- [5] C. Duan, T. E. Rook, R. Singh, *Sub-harmonic resonance in a nearly pre-loaded mechanical oscillator*, Nonlinear Dynamics, Vol. 50, No. 3, Springer (2007), pp. 639-650.
- [6] A. Bourdon, K. Yakhou, L. Chaloyard, D. Play, L. B. Insa, *Influence of the mechanical architecture and coupling effects on the vibratory behavior of complex gear transmissions*, Proceedings of ASME Design Engineering Technical Conferences, Vol. 99, American Society of Mechanical Engineers (1999), pp. 12–15.
- [7] P. Novotny, V. Pistek, *New efficient methods for powertrain vibration analysis*, Proceedings of the Institution of Mechanical Engineers, Part D: Journal of Automobile Engineering, Vol. 2010, No. 224, SAGE (2010), pp. 611-629.
- [8] MD ADAMS 2011, *Online Help*, MSC Software, California (2011).
- [9] CATIA v5, *Online Help*, Dassault Systèmes, Vélizy-Villacoublay (2010).
- [10] ANSA v13, *Online Help*, BETA CAE Systems, Thessaloniki (2011).
- [11] MSC NASTRAN 2012, *Quick Reference Guide*, MSC Software, California (2011).
- [12] G. Ottarson, G. Moore, D. Minen, *MDI/ADAMS-MSC/NASTRAN Integration Using Component Mode Synthesis*, MSC Americas Users' Conference (1998).
- [13] L. Houpert, *A uniform analytical approach for ball and roller bearings calculations*, Journal of Tribology, Vol. 119, American Society of Mechanical Engineers (1997), p. 851.
- [14] M. Zink, M. Hausner, *The Centrifugal Pendulum-type Absorber - Application, Performance and Limits of Speed-adaptive Absorbers*, ATZ-worldwide, Vol. 111, No. 8, ATZ (2009), pp. 42-47.
- [15] Swedish Standard SS1864, *Helical gears - Geometrical data*, Issue 5, Standardiseringskommissionen i Sverige, Stockholm (1978).
- [16] Swedish Standard SS1871, *Spur and helical gears - Calculation of load capacity*, Issue 3, Standardiseringskommissionen i Sverige, Stockholm (1978).

-
- [17] Swedish Standard SS1862, *Bevel gears - Calculation of load capacity*, Issue 3, Standardiseringskommissionen i Sverige, Stockholm (1978).
- [18] S. Adamson, *Improved Approaches to the Measurement and Analysis of Torsional Vibration*, SAE Technical Paper 2004-01-1723, SAE International (2004).
- [19] C. E. Shannon, *Communication in the presence of noise*, Proceedings of the IEEE, Vol. 86, No. 2, Institute of Electrical and Electronics Engineers (1998), pp. 447–457.
- [20] G. B. Folland, *Fourier analysis and its applications*, Mathematics Series, Brooks/Cole, California (1992).
- [21] J. R. Blough, *Understanding Order Tracking Algorithm Limitations*, SAE Technical Paper 2009-01-2157, SAE International (2009).
- [22] G. E. P. Box, J. S. Hunter, W. G. Hunter, *Statistics for Experimenters: Design, Innovation, and Discovery*, 2nd edition, Wiley-Interscience, New Jersey (2005).
- [23] G. Genta, *Dynamics of Rotating Structures*, Mechanical Engineering Series, Springer (2005).
- [24] Matlab R2010b, *Online Help*, MathWorks, Natick (2010).

